Pure spin squeezing of *h*-BN spins coupled to superconducting resonator

Yi-Fan Qiao,[1,2] Jia-Qiang Chen,[1] Yuan Zhou,[3] Peng-Bo Li,[1,*] and Wei-Bo Gao[2,†]

[1]*Ministry of Education Key Laboratory for Nonequilibrium Synthesis and Modulation of Condensed Matter, Shaanxi Province Key Laboratory of Quantum Information and Quantum Optoelectronic Devices, School of Physics, Xi'an Jiaotong University, Xi'an 710049, China*

[2]*Division of Physics and Applied Physics, School of Physical and Mathematical Sciences, Nanyang Technological University, Singapore 637371, Singapore*

[3]*School of Mathematics, Physics and Optoelectronic Engineering, Hubei University of Automotive Technology, Shiyan 442002, China*

(Received 21 December 2022; accepted 2 May 2023; published 18 May 2023)

The negatively charged boron vacancy (VB^-) spin defect in two-dimensional (2D) hexagonal boron nitride (*h*-BN) has attracted much attention for potential applications in quantum photonics recently. Its inherent van der Waals force mechanism guarantees convenient heterostructures for quantum sensing. By virtue of such materials, researchers not only can fabricate enough thin spin film naturally close to the sensing target but also can prepare an almost perfect spin ensemble with a uniform orientation. We here propose a setup with an ensemble of VB^- spins strongly coupled to the superconducting coplanar waveguide resonator through the magnetic-dipolar interaction. The collective coupling strength is predicted to be $G/2\pi \sim 15$ MHz, which corresponds to the strong coupling region. This collective spin-photon interaction can mimic the one-axis twisting Lipkin-Meshkov-Glick model effectively and therefore guarantee the dynamic generation of the spin-squeezed state. In addition, we show the influence of inhomogeneous coupling caused by sample thickness on squeezing, which proves the validity of the homogeneity assumption in our scheme. This attempt not only explores the possibility and superiority of 2D VB^- spins but also opens another avenue for quantum hybridization.

DOI: 10.1103/PhysRevB.107.195425

I. INTRODUCTION

Spin squeezing means that the fluctuation of the quantum state is lower than the standard quantum limit [1–6]; it plays an important role in the field of quantum information and quantum metrology [7–17]. Currently, spin squeezing has been generated in many systems using the dynamic method [18–25] and reservoir engineering [26–35]. Although great progress has been achieved, there is still a considerable challenge to overcome. Spin defects in traditional three-dimensional (3D) crystal always have multiple spin orientations [36–39], which results in inhomogeneous frequency and interaction and leads to great obstacles to the alignment of magnetic field in experiments. In addition, these schemes always require an auxiliary cavity [40–42], but the distribution of the cavity field is usually inhomogeneous, resulting in inhomogeneous coupling strength. These intrinsic limitations of the defect center in 3D materials will directly restrict its further application to quantum metrology.

Recently, the two-dimensional (2D) insulator material hexagonal boron nitride (*h*-BN) has attracted much attention for studying light-matter interactions at the nanoscale [43–49]. In contrast to conventional bulk materials, the 2D layered structure of *h*-BN has many outstanding features; that is, it is more suitable for implanting, fabricating, and integrating with photonic chips. Specifically, an important spin defect, namely, the negatively charged boron vacancy (VB^-) in *h*-BN, has become a hot topic of investigation. We note this type of solid-state spin is quite similar to nitrogen vacancy center in diamond. First, VB^- spin possesses D_{3h} point-group symmetry [50–53], which gives rise to a triplet ground state with a zero-field splitting of $\sim 2\pi \times 3.5$ GHz. Second, it can be initialized, manipulated, and read out via the optical method [54–58]. Third, the VB^- spin defect is more convenient to scale up according to realistic requirements, and recent experiments also demonstrated that it can be deterministically created using various means, such as neutron irradiation, ion implantation, and electron irradiation [58–61]. Finally, VB^- spins in *h*-BN have an almost uniform orientation which is perpendicular to the layer plane, and this important feature is superior to the other color centers in bulk materials. Therefore, VB^- spin in *h*-BN has triggered a plethora of studies in high-resolution sensing and imaging [62–67].

In this paper, we propose a hybrid device in which an ensemble of VB^- spins is magnetically coupled to a half-wavelength superconducting coplanar waveguide (CPW) resonator. The *h*-BN crystal ($200 \times 20 \times 10\,\mu m^3$), containing $N \sim 2.16 \times 10^{10}$ VB^- spins, is attached to the middle of the central conductor. The magnetic field in this region can approximately be treated as a homogeneous field with a magnitude value of 3.7 nT. An external magnetic field perpendicular to the conductor surface is applied to modify the frequency of the Zeeman splitting, with the purpose of

*lipengbo@mail.xjtu.edu.cn
†wbgao@ntu.edu.sg

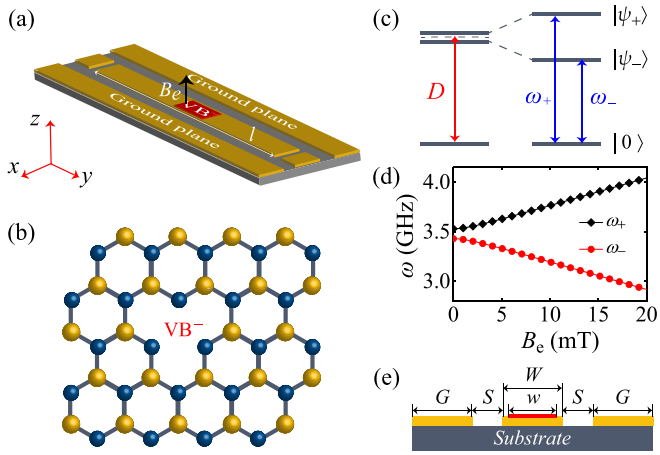

FIG. 1. (a) Schematic of an ensemble of VB^- spins glued on top and in the middle of a CPW resonator. A static magnetic field $\mathbf{B}_e$ is applied parallel to the c axis of the h-BN crystal. (b) Sketch of the negatively charged boron vacancy defect. Boron atoms and nitrogen atoms are represented by yellow and blue spheres, respectively. (c) The level structure of the electronic ground state of the VB^- spin defect. (d) Frequency splitting of the VB^- spin states as a function of the external magnetic field. (e) Cross-sectional sketch and geometrical parameters of the CPW resonator.

ensuring the resonance condition matches the CPW resonator. In this case, the coupling strength of a single VB^- spin coupled to the CPW resonator is estimated as $g \sim 2\pi \times 100$ Hz, and the collective coupling strength of the VB^- ensemble can reach $G = g\sqrt{N} \approx 2\pi \times 15$ MHz, which also potentially provides a different 2D strong coupling platform or interface. As an intriguing application, we show how to use our setup to generate the spin-squeezed state (SSS). Under the condition of large detuning, we can obtain the nonlinear spin-spin interactions using the Schrieffer-Wolff transformation, which can be further reduced to the one-axis twisting Lipkin-Meshkov-Glick (LMG) Hamiltonian. The degree of generated spin squeezing scales as $N^{-0.7}$ in the absence of decoherence. In addition, we discuss the influence of magnetic-field inhomogeneity on squeezing and prove the validity of the homogeneity assumption in our scheme. Our work constitutes a step forward in exploring the possibility and superiority of VB^- spins in a 2D h-BN crystal interacting with other quantum systems.

II. MODEL

In the setup depicted in Fig. 1(a), a h-BN crystal containing the VB^- spins is glued on the top of a half-wavelength CPW resonator. The negatively charged boron vacancy is formed by a missing boron atom replaced by an extra electron and three surrounding equivalent nitrogen atoms in the h-BN lattice, as schematically shown in Fig. 1(b). It has a triplet electronic ground state ($S = 1$) with a separation of $D \approx 2\pi \times 3.5$ GHz between states $m_S = 0$ and $m_S = \pm 1$. In the presence of an external magnetic field, the two upper spin states can be split and shifted due to the Zeeman effect, and the corresponding simplified energy level diagram is shown in Fig. 1(c). We assume the magnetic field $\mathbf{B}_e = B_e\mathbf{e}_z$, where the z-coordinate axis coincides with the c axis of the h-BN crystal. In this case, the spin Hamiltonian for a single VB^- spin can be represented by ($\hbar = 1$)

$$\hat{H}_{\rm VB} = \omega_-|\psi_-\rangle\langle\psi_-| + \omega_+|\psi_+\rangle\langle\psi_+|, \tag{1}$$

where $\omega_\pm = D \pm \sqrt{E^2 + (g_{\rm VB}\mu_{\rm B}B_e)^2}$ are frequency splittings of eigenstates $|\psi_\pm\rangle$ relative to $|0\rangle$ [shown in Fig. 1(d)]. D and E are zero-field splitting parameters. $g_{\rm VB} = 2$ and $\mu_{\rm B}/h = 14$ MHz/mT are the Landé factor and Bohr magneton, respectively.

The CPW resonator consists of a central conductor plus two ground planes, which are fabricated on a dielectric substrate [68–71]. Its electromagnetic fields are strongly confined near the gaps between the central conductor and ground planes [68,72]. It can be modeled as a single-model harmonic oscillator, and the free Hamiltonian is given by $\hat{H}_R = \omega_R\hat{a}^\dagger\hat{a}$, where $\hat{a}$ ($\hat{a}^\dagger$) is the annihilation (creation) operator and ω_R is the resonant frequency of the resonator mode. The quantized resonator magnetic field can be described by $\hat{\mathbf{B}}(\mathbf{r}) = \mathbf{B}_0(\mathbf{r})(\hat{a} + \hat{a}^\dagger)$, where $\mathbf{B}_0(\mathbf{r})$ is the magnetic field of a single microwave photon generated by the vacuum fluctuations at position $\mathbf{r}$ [71,72]. A single VB^- spin at $\mathbf{r}_n$ is coupled to the quantized resonator field through the magnetic-dipolar interaction, and the interaction Hamiltonian has the form $\hat{H}_{\rm int} = g_{\rm VB}\mu_B\hat{\mathbf{B}}(\mathbf{r}_n)\cdot\hat{\mathbf{S}}_n$, where $\hat{\mathbf{S}}_n = (\hat{S}_x^n, \hat{S}_y^n, \hat{S}_z^n)$ are spin operators. Assuming $\mathbf{B}_0(\mathbf{r}) \parallel \mathbf{e}_x$, the Hamiltonian for the whole system reads

$$\hat{H} = \omega_R\hat{a}^\dagger\hat{a} + \sum_n \hat{H}_{\rm VB}^{(n)} + \sum_{n,\alpha=\pm} g_n(\hat{a} + \hat{a}^\dagger)|0\rangle_n\langle\psi_\alpha| + \text{H.c.}, \tag{2}$$

where n labels the VB^- spin located at positions $\mathbf{r}_n = (x_n, y_n, z_n)$ and the coupling $g_n = g_{\rm VB}\mu_B B_x(\mathbf{r}_n)$.

III. THE MAGNETIC COUPLING

As shown in Fig. 1(e), we consider a resonator with the size $(W, G, S) = (50\,\mu\text{m}, 50\,\mu\text{m}, 25\,\mu\text{m})$, which corresponds to a characteristic impedance of $Z_0 \approx 50\,\Omega$. The resonator length $l = \lambda/2 = 2.1$ cm is designed so that the fundamental resonance frequency $\omega_R = \pi c/l\sqrt{\epsilon_{\rm eff}} \approx 2\pi \times 3.05$ GHz is in resonance with the VB^- defects [73,74]. Here, λ is the mode wavelength, c is the vacuum speed of light, and $\epsilon_{\rm eff} = 5.5$ is the effective dielectric constant. We display the transverse magnetic field of a single photon in the cross section of the coplanar waveguide in Figs. 2(a) and 2(b). Compared to the transverse magnetic-field components $B_{x,z}(\mathbf{r})$, the longitudinal component $B_y(\mathbf{r})$ is so weak that it can be neglected. On the top of the central conductor, the magnetic strength varies slowly, and the direction is almost parallel to $\mathbf{e}_x$. More specifically, we consider the distribution of magnetic-field strength for fixed x or z in Figs. 2(c) and 2(d). The magnetic field can be regarded as a constant in the range of $|x| \leqslant 10\,\mu$m and $z \leqslant 10\,\mu$m. In this case, we choose a VB^- sample with the size $V = 200 \times 20 \times 10\,\mu\text{m}^3$ to make the coupling homogeneous. When the VB^- ensemble is placed near the antinode of the field, the wavelength λ is much larger than the spatial dimension of the VB^- ensemble. We thus neglect the change in the magnetic microwave field over the size of the h-BN crystal

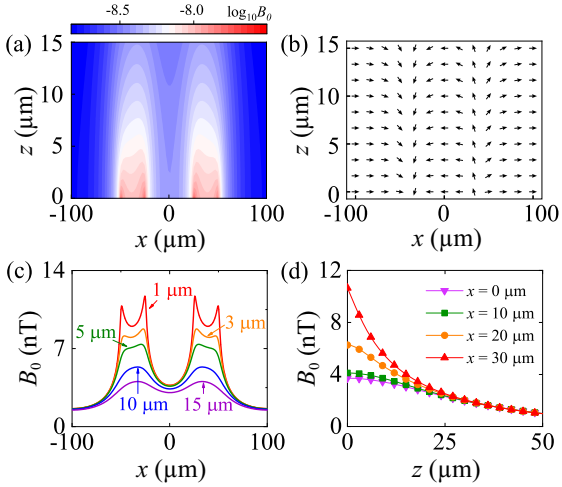

FIG. 2. The transverse magnetic field of a single photon above the CPW resonator. (a) The contour maps of magnetic-field strength versus positions x and z. (b) Vector plot of the magnetic field in the resonator. (c) Magnetic-field strength along the x direction for different distances above the resonator surface. (d) Magnetic-field strength as a function of distance to the resonator surface at the central conductor ($y = 0,\ 10,\ 20\,\mu$m) and at the gap ($y = 30\,\mu$m).

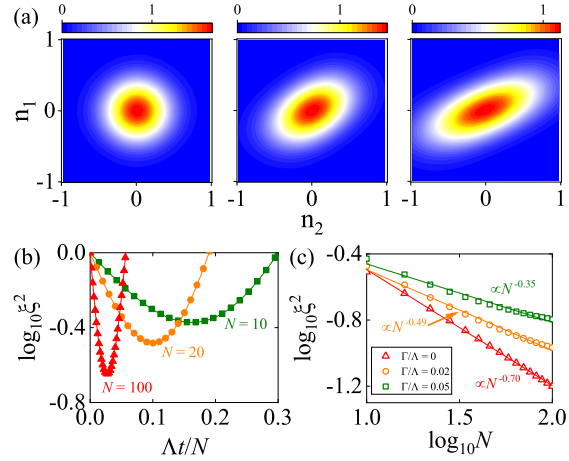

FIG. 3. (a) Spin Husimi Q function in the plane perpendicular to the mean spin direction $\mathbf{n}_0$ with $\Lambda t/N = 0$, $\Lambda t/N = 0.05$, and $\Lambda t/N = 0.1$. (b) The evolution of the spin squeezing parameter with $N = 10,\ 20,\ 100$. (c) The optimal squeezing versus the number of spins with different collective decay rates. The solid line is the numerical fitting, and it gives $\xi^2 \sim N^{-0.7}$ in the absence of decoherence.

and get $\mathbf{B}(\mathbf{r}_n) \approx \bar{B}_0\mathbf{e}_x$, with $\bar{B}_0 \approx 3.7\,$nT, for all defects. So far, we can rewrite the total Hamiltonian as

$$\hat{H} = \omega_R\hat{a}^\dagger\hat{a} + \sum_n(\omega_-|\psi_-\rangle_n\langle\psi_-| + \omega_+|\psi_+\rangle_n\langle\psi_+|) + g(\hat{a} + \hat{a}^\dagger)\sum_n(|0\rangle_n\langle\psi_-| + |0\rangle_n\langle\psi_+| + \text{H.c.}), \quad (3)$$

where $g = g_{\text{VB}}\mu_B\bar{B}_0 \approx 2\pi \times 100\,$Hz is the coupling strength for a single VB^- spin. For the VB^- ensemble, an effective method to generate the VB^- spin experimentally is through neutron irradiation [58], which results in a defect density of $\rho \approx 5.4 \times 10^{17}\,\text{cm}^{-3}$. From this we find the coherent collective coupling strength is $G = g\sqrt{N} \approx 2\pi \times 15\,$MHz, with $N = \rho V \approx 2.16 \times 10^{10}$ being the number of VB^- defects, which is larger than the resonator decay κ and the spin relaxation Γ_ϕ and thus reaches the strong coupling regime.

IV. ONE-AXIS TWISTING MODEL

We next consider generating entangled states with this setup. Assuming that the resonator frequency ω_R is near resonance with ω_-, the Hamiltonian can be simplified to a Tavis-Cummings form in the rotating-wave approximation,

$$\hat{H} = \omega_R\hat{a}^\dagger\hat{a} + \omega_-\hat{J}_z + \frac{G}{\sqrt{N}}(\hat{a}\hat{J}^\dagger + \hat{a}^\dagger\hat{J}), \quad (4)$$

where $\hat{J}_z = \frac{1}{2}\sum_n|\psi_-\rangle_n\langle\psi_-| - |0\rangle_n\langle 0|$ and $\hat{J} = \sum_n|0\rangle_n\langle\psi_-|$ are the collective spin operators satisfying the usual angular momentum commutation relations. In the limit of the large-detuning condition $G \ll \Delta = \omega_- - \omega_R$, we obtain an effective Hamiltonian which describes the nonlinear spin-spin interaction through a Schrieffer-Wolff transformation [1,75], $\hat{H}_S = e^{-\hat{S}}\hat{H}e^{\hat{S}}$, with $\hat{S} = \frac{g}{\Delta}(\hat{J}\hat{a}^\dagger - \hat{J}^\dagger\hat{a})$. Keeping terms to the second order, the effective Hamiltonian is given by

$$\hat{H}_S = \omega_R\hat{a}^\dagger\hat{a} + \left(\omega_- + \frac{2\Lambda}{N}\hat{a}^\dagger\hat{a}\right)\hat{J}_z + \frac{\Lambda}{N}\hat{J}^\dagger\hat{J}, \quad (5)$$

where $\Lambda = G^2/\Delta$ is the spin-spin coupling strength. The operator $\hat{J}^\dagger\hat{J}$ can be rewritten as $\hat{\mathbf{J}}^2 - \hat{J}_z^2 + \hat{J}_z$ [1,19]. Because the total spin $\hat{\mathbf{J}}^2$ commutes with the Hamiltonian $\hat{H}_S$, the system evolves within the manifold of $J = N/2$ if the initial state is prepared in the maximally polarized state $|J = N/2, J_x = N/2\rangle$. Assuming the thermal phonon number $n_{\text{th}} \sim 0$, Hamiltonian (5) in the interaction picture is written as

$$\hat{H}_S = -\frac{\Lambda}{N}\hat{J}_z^2, \quad (6)$$

which corresponds to the one-axis twisting Hamiltonian [18] and can be used to generate SSS. We define the density operator $\hat{\rho}$ to describe the VB^- degrees of freedom, and the motion of $\hat{\rho}$ is controlled by the following master equation:

$$\dot{\hat{\rho}} = -i[\hat{H}_S, \hat{\rho}] + \frac{\Gamma}{N}\mathcal{D}[\hat{J}]\hat{\rho}, \quad (7)$$

where $\mathcal{D}[\hat{o}]\hat{\rho} = \hat{o}\hat{\rho}\hat{o}^\dagger - \frac{1}{2}(\hat{o}^\dagger\hat{o}\hat{\rho} + \hat{\rho}\hat{o}^\dagger\hat{o})$ and $\Gamma = \kappa G^2/\Delta^2$ is the collective decay rate induced by the resonator and the spin relaxation is assumed to be zero.

Spin squeezing means the fluctuation in a certain spin component is suppressed below the standard quantum limit [18–20]. In order to visually characterize the spin squeezing, we introduce Husimi Q function, $Q(\theta,\phi) = (2j+1)/(4\pi)\langle\theta,\phi|\hat{\rho}|\theta,\phi\rangle$, where $|\theta,\phi\rangle = (1+|\eta|^2)^{-j}e^{-\eta^*\hat{J}}|j,j\rangle$, with $|j,m\rangle$ ($j = N/2$ and $m = -j,\ldots,j$) being the eigenstates of $\{\hat{\mathbf{J}}^2, \hat{J}_z\}$ and $\eta = -\tan(\theta/2)e^{-i\phi}$ (θ and ϕ are the polar and azimuthal angles) [28,76]. In Fig. 3(a), we display the projections of the Q function on the $(\mathbf{n}_1, \mathbf{n}_2)$ plane at three different moment for $N = 20$. Husimi Q function at the initial time $\Lambda t/N = 0$ is a circle, which corresponds to the coherent spin state $|\Psi_0\rangle = |J = N/2, J_x = N/2\rangle$. It gradually becomes squeezed and elliptical as the time

increases, while the squeezing angle rotates. Eventually, the optimal squeezing is reached at $\Lambda t/N = 0.1$. In addition, we also introduce the spin squeezing parameter [5] to quantify the degree of spin squeezing

$$\xi^2 = \frac{N \min\left(\Delta \hat{J}^2_{\mathbf{n}_\perp}\right)}{|\langle \hat{\mathbf{J}} \rangle|^2}, \tag{8}$$

where $\mathbf{n}_\perp$ is an axis perpendicular to the mean spin direction $\mathbf{n}_0 = \mathrm{Tr}(\hat{\rho}\hat{\mathbf{J}})/|\mathrm{Tr}(\hat{\rho}\hat{\mathbf{J}})|$ [28]. When $\xi^2 < 1$, the state is squeezed. The evolution of the squeezing parameter is shown in Fig. 3(b) for $N = 10,\ 20,\ 100$. As we expect, the time to reach the optimal squeezing is reduced to $t_{\mathrm{opt}} \propto 1/N$ due to the collective effect. In Fig. 3(c), we plot the optimal squeezing versus the spin number N for different collective decay rates. The spin squeezing scales as $N^{-0.7}$ in the absence of decoherence. With a modest quality factor $Q = 10^3$, it still produces considerable squeezing, which is shown in the orange circle in Fig. 3(c).

V. VALIDITY OF THE HOMOGENEITY ASSUMPTION

In our scheme, we assume that the magnetic field is uniform in the whole spin ensemble, so we get a homogeneous coupling strength. But in fact, the magnetic field is nonuniform, as shown in Fig. 2. Here, we investigate the influence of the inhomogeneous coupling caused by the magnetic field on the squeezing with different thicknesses h. As the computational complexity increases exponentially with the spin number, we here investigate a system consisting of six spins without decoherence, in which the coupling strength of each spin is given by $g_n(\mathbf{r}) = g_{\mathrm{VB}}\mu_B B_x(z_n)$. We assume that these six spins are uniformly distributed between $(0, 0, 0)$ and $(0, 0, h)$. The dependence of the magnetic-field strength on coordinate z is shown by the purple inverted triangles in Fig. 2(d), and the corresponding coupling strength of each spin can be calculated. Then the Hamiltonian is given by

$$H = \sum_n \left(\frac{\Delta}{2} + \frac{g_n^2(z_n)}{\Delta}\hat{a}^\dagger\hat{a}\right)\hat{\sigma}_n^z + \sum_{n,m}\frac{g_n(z_n)g_m(z_m)}{\Delta}\hat{\sigma}_n^\dagger\hat{\sigma}_m, \tag{9}$$

where $\hat{\sigma}_n^z = |\psi_-\rangle_n\langle\psi_-| - |0\rangle_n\langle 0|$ is the Pauli operator and $\hat{\sigma}_n = |0\rangle_n\langle\psi_-|$ is the single-spin lowering operator. If the assumption of homogeneity is valid in our scheme, we should see that the squeezing is almost constant at $h < 10\,\mu$m.

In Fig. 4(a), we display the evolution of the squeezing parameter ξ^2 with three different thicknesses, $h = 10,\ 50,\ 100\,\mu$m. For the small thickness, $h = 10\,\mu$m, the system exhibits significant squeezing. As the thickness increases, the optimal squeezing is reduced, and the time to reach the optimal squeezing is extended. To further discuss the impact of thickness on optimal squeezing, we plot the optimal squeezing versus sample thickness h ranging from 0 to 100 μm in Fig. 4(b). When the thickness $h = 0$, these six spins have the same coupling strength (homogeneous case) and exhibit the strongest squeezing. When the thickness h is less than 10 μm (the blue shading), the influence of thickness on optimal squeezing is so slight that the change in the numerical value is almost invisible, which verifies that the previous assumption of homogeneous coupling in our setup is valid. When the thickness h is greater than 10 μm (the yellow shading), the optimal squeezing shows a strong dependence on the thickness h, and the squeezing degree decreases rapidly.

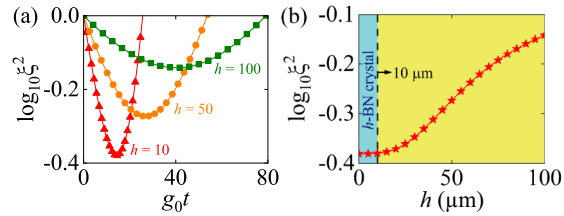

FIG. 4. (a) Evolution of the spin squeezing parameter with three different thicknesses, $h = 10,\ 50,\ 100\,\mu$m, for spin number $N = 6$ without decoherence. $g_0 = g(0)$ is the spin-photon coupling strength of the spin at position $(0,\ 0,\ 0)$. (b) The optimal squeezing parameter versus the thickness. The black dashed line, corresponding to $h = 10\,\mu$m, separates the blue shading (corresponding to VB^- spins in our setup) from the yellow shading.

VI. FEASIBILITY

In order to examine the feasibility of this scheme in experiment, we now discuss the relevant parameters. A static external magnetic field $B_e = 10$ mT is applied to the VB^- spin, resulting in the spin frequency $\omega_- \approx 2\pi \times 3.2$ GHz of state $|\psi_-\rangle$. The frequency of the CPW resonator is given by $\omega_R = \pi c/l\sqrt{\epsilon_{\mathrm{eff}}} \approx 2\pi \times 3.05$ GHz. The detuning between the spin and the CPW resonator is $\Delta = \omega_- - \omega_R \approx 2\pi \times 150$ MHz, which is larger than the collective coupling strength $G = 2\pi \times 15$ MHz and satisfies the large-detuning limit. The spin dephasing rate is $\Gamma_\phi = 1/T_2 \sim 2\pi \times 80$ kHz, and the resonator decay rate is $\kappa = \omega_R/Q$. Even under a modest quality factor $Q = 10^3$, the cooperativity $C = g^2/\kappa\Gamma_\phi$ is still greater than 1, indicating a strong coupling regime. After a series of transformations and approximations, we get the effective spin-spin coupling strength $\Lambda = G^2/\Delta = 2\pi \times 1.5$ MHz and the collective decay $\Gamma = \kappa G^2/\Delta^2 \sim 0.02\Lambda$ of the spin ensemble induced by the CPW resonator. Even stronger dissipation Γ causes only a slight reduction in squeezing, as shown in Fig. 3(c). The only problem may be spin decoherence. A large number of nuclear spins around the defect introduce an equivalent random local magnetic field, also known as the Overhauser field, resulting in an extremely short spin dephasing time $T_2^* \approx 100$ ns [53,54]. However, dynamical decoupling can eliminate this effect [77], and the spin coherence time $T_2 \approx 2\,\mu$s [54,66] has been measured experimentally. The optimal time $t_{\mathrm{opt}} \sim 2/\Lambda \approx 0.21\,\mu$s of spin squeezing is less than the spin coherence time T_2, so we predict that we can get reduced squeezing. Research on extending the VB^- coherence time, such as applying an enhanced magnetic field [78], is in progress.

VII. CONCLUSION

Through a theoretical study of the magnetic coupling between the VB^- spins and CPW resonator, we first estimated that its coherent coupling strength at a single quantum level is $g/2\pi \sim 100$ Hz and therefore achieved pin-photon interactions with the collective and strong coupling strength $G/2\pi \sim 15$ MHz. In one potential application of this hybrid design, these collective spins can be engineered into the SSS. h-BN

can be very thin down to atomic layer thickness, ensuring it is close to the superconducting resonator and therefore guaranteeing homogeneous coupling. As a result, we get strong spin squeezing, which shows the potential of VB^- in the application of quantum metrology and quantum sensing. The high density of VB^- spins was produced in a recent experiment by means of neutron irradiation, which allowed us to achieve a stronger collective coupling to the microwave photons. Therefore, it is necessary and meaningful for us to study such a hybrid system, and we also note that this attempt could also open an avenue for others feasible schemes for VB^- spins coupled to other quantum systems.

ACKNOWLEDGMENTS

This work is supported by the National Natural Science Foundation of China (Grant No. 92065105), the Natural Science Basic Research Program of Shaanxi (Program No. 2020JC-02), the National Research Foundation, Singapore, and A*STAR under its Quantum Engineering Programme (Grants No. NRF2021-QEP2-03-P01, No. NRF2021-QEP2-03-P10, and No. NRF2021-QEP2-01-P01). Y.Z. is supported by the Natural Science Foundation of Hubei Province (Grant No. 2020CFB748) and the Natural Science Foundation of Shandong Province (Grants No. ZR2021MA042 and No. ZR2021MA078).

APPENDIX A: MODELING OF N VB^- SPINS COUPLED TO A RESONATOR

As described in the main text, a h-BN flake containing an ensemble of VB^- defects is stuck on a superconducting CPW resonator. The total Hamiltonian for this system contains three parts, which can be represented by

$$\hat{H} = \hat{H}_{\rm VB} + \hat{H}_R + \hat{H}_{\rm int}. \tag{A1}$$

The first part is the Hamiltonian of the VB^- ensemble; the second part is the Hamiltonian of the CPW resonator, and the last part is the coupling between the VB^- ensemble and the resonator. We provide a detailed discussion of these three parts in the following.

1. Electronic structure of the VB^- defect

The negatively charged VB^- defect is formed by a missing boron atom replaced by an extra electron and three surrounding equivalent nitrogen atoms in the h-BN lattice. It can be experimentally generated by means of neutron irradiation, ion implantation, and electron irradiation. The electrons of VB^- spin occupy the defect states, so that the dangling bond state becomes half occupied and gives rise to a spin-1 ground state [52,54]. The Hamiltonian describing the spin-spin interaction of the VB^- defect can be represented as

$$\hat{H}_{\rm VB} = D\left[\hat{S}_z^2 - S(S+1)/3\right] + E\left(\hat{S}_x^2 - \hat{S}_y^2\right) + g_{\rm VB}\mu_B B_e \hat{S}_z, \tag{A2}$$

where D and E are the zero-field splitting parameters due to spin-spin interaction and residual strain in the crystal, respectively. $\hat{\mathbf{S}} = (\hat{S}_x, \hat{S}_y, \hat{S}_z)$ are the total spin $S = 1$ operators of the VB^- defect. The last term is the Zeeman splitting, and we have assumed the external magnetic field $\mathbf{B}_e = B_e\mathbf{e}_z$, which is parallel to the c axis of the h-BN lattice. $g_{\rm VB} = 2$ and $\mu_{\rm B}/h = 14$ MHz/mT are the Landé factor and Bohr magneton, respectively. In the basis of eigenstates of $\hat{S}_z$, the Hamiltonian $\hat{H}_{\rm VB}$ in Eq. (A2) can be written in the following matrix form:

$$\hat{H}_{\rm VB} = \begin{bmatrix} D + g_{\rm VB}\mu_B B_e & 0 & E \\ 0 & 0 & 0 \\ E & 0 & D - g_{\rm VB}\mu_B B_e \end{bmatrix}. \tag{A3}$$

Diagonalizing Eq. (A3), we can obtain the eigenstates

$$\begin{aligned} |\psi_0\rangle &= |0\rangle, \\ |\psi_-\rangle &= \sin\frac{\theta}{2}|+1\rangle - \cos\frac{\theta}{2}|-1\rangle, \\ |\psi_+\rangle &= \cos\frac{\theta}{2}|+1\rangle + \sin\frac{\theta}{2}|-1\rangle, \end{aligned} \tag{A4}$$

where $\tan\theta = \frac{E}{g_{\rm VB}\mu_B B_e}$ and the corresponding eigenfrequencies are

$$\omega_0 = 0,\ \omega_\pm = D \pm \sqrt{E^2 + (g_{\rm VB}\mu_B B_e)^2}. \tag{A5}$$

Then we have the Hamiltonian (1) in the main text.

2. Magnetic-dipolar interaction

The resonator used in our setup is a half-wavelength ($\lambda/2$) transmission line resonator based on a superconducting coplanar waveguide. A CPW resonator consists of a center conductor with width W and two neighboring ground planes with width G; the gap width between the center conductor and the ground plane is represented by S. The characteristic impedance Z_0 of the CPW resonator depends on the ratio of W/S, which is designed so that the resonator has a minimal radiation loss with $\sim 50\,\Omega$ impedance. The resonator frequency ω_m is related to the resonator length l, which is calculated by the equation $\omega_m = m\pi c/l\sqrt{\epsilon_{\rm eff}}$, where c is the vacuum speed of light and $\epsilon_{\rm eff} = 5.5$ is the effective dielectric constant. The coplanar waveguide problem is reduced to a rectangular waveguide problem by inserting electric walls at $y = -l/2$ and $y = l/2$ and a magnetic wall at $x = b$. The classical magnetic-field components $\mathbf{B}_0(\mathbf{r}) = \mu_0\mathbf{H}(\mathbf{r})$ can be calculated by

$$\begin{aligned} H_x &= \frac{\varepsilon_0}{\eta}\frac{\lambda_0}{\lambda}\sum_{n>0}\frac{1}{F_n}\left[\frac{\sin n\pi\delta/2}{n\pi\delta/2}\sin\frac{n\pi\bar{\delta}}{2}\right] \\ &\quad\times \cos\frac{n\pi x}{b}e^{-\gamma_n|z|}\cos\frac{m\pi y}{l}, \\ H_y &= -i\frac{\varepsilon_0}{\eta}\left(\frac{\lambda_0}{\lambda}\right)^2\frac{2b}{\lambda_0}\sum_{n>0}\frac{1-(\lambda/\lambda_0)^2}{nF_n}\left[\frac{\sin n\pi\delta/2}{n\pi\delta/2}\sin\frac{n\pi\bar{\delta}}{2}\right] \\ &\quad\times \sin\frac{n\pi x}{b}e^{-\gamma_n|z|}\cos\frac{m\pi y}{l}, \\ H_z &= \frac{\varepsilon_0}{\eta}\frac{\lambda_0}{\lambda}\sum_{n>0}\left[\frac{\sin n\pi\delta/2}{n\pi\delta/2}\sin\frac{n\pi\bar{\delta}}{2}\right] \\ &\quad\times \cos\frac{n\pi x}{b}e^{-\gamma_n|z|}\cos\frac{m\pi y}{l}, \end{aligned} \tag{A6}$$

where $\varepsilon_0 = \sqrt{\hbar\omega_R/\epsilon_0 V_c}$, $\delta = S/b$, $\bar{\delta} = (S+w)/b$, $\eta = 377\,\Omega$, and $F_n = (b\gamma_n/n\pi) = \sqrt{1+(2b/n\lambda)^2[(\lambda_0/\lambda)^2-1]}$ [79–81]. Here, we choose the resonator length $l = 2.1$ cm, which corresponds to a fundamental frequency of $\sim 2\pi \times 3.05$ GHz to ensure the resonance condition. $\lambda = 2l$ is the cavity wavelength, and λ_0 is the free space wavelength, expressed as $\lambda_0 = \lambda\sqrt{\epsilon_{\text{eff}}}$.

Following the standard procedure for quantizing the electromagnetic fields, we obtain the quantized form of the single-mode magnetic-field operator for the CPW cavity:

$$\hat{\mathbf{B}}(\mathbf{r},t) = \mathbf{B}(\mathbf{r})(\hat{a}e^{-i\omega_R t} + \hat{a}^\dagger e^{i\omega_R t}), \tag{A7}$$

where $\mathbf{B}(\mathbf{r}) = \mu_0(H_x, H_y, H_z)$. The CPW Hamiltonian and magnetic-dipolar interaction are written as

$$\hat{H}_R = \omega_R \hat{a}^\dagger \hat{a}, \tag{A8}$$

$$\hat{H}_{\text{int}} = g_{\text{VB}}\mu_B \hat{\mathbf{B}}(\mathbf{r}_n)\cdot\hat{\mathbf{S}}_n, \tag{A9}$$

where n labels the VB^- spin located at positions $\mathbf{r}_n = (x_n, y_n, z_n)$ and $\hat{\mathbf{S}}_n = (\hat{S}_x^n, \hat{S}_y^n, \hat{S}_z^n)$ are spin operators. The magnetic-field operator in the position of the VB^- can be written as $\hat{\mathbf{B}}(\mathbf{r}) = \mathbf{B}_0(\mathbf{r})(\hat{a}+\hat{a}^\dagger)$. The longitudinal component B_y can be ignored since it is always small. In Fig. 2 in the main text, we showed the transverse magnetic field of a single photon in the cross section of the coplanar waveguide. From the vector plot, the magnetic field can be considered to be parallel to the x axis in the range of the spin ensemble. We find that the magnetic field in this region can be regarded as a uniform magnetic field with $\mathbf{B}_0(\mathbf{r}) \sim \bar{B}_0\mathbf{e}_x$, so the interaction Hamiltonian is reduced to

$$\hat{H}_{\text{int}} = g(\hat{a}+\hat{a}^\dagger)\hat{S}_x, \tag{A10}$$

where $g = g_{\text{VB}}\mu_B\bar{B}_0$ is single-spin coupling strength. In the basis of new eigenvectors $\{|0\rangle, |\psi_\pm\rangle\}$, the total Hamiltonian of the whole spin ensemble has the form

$$\hat{H} = \omega_R\hat{a}^\dagger\hat{a} + \sum_n \hat{H}_{\text{VB}}^{(n)} + \sum_{n,\alpha=\pm} g_n(\hat{a}+\hat{a}^\dagger)(|0\rangle_n\langle\psi_\alpha| + |\psi_\alpha\rangle_n\langle 0|). \tag{A11}$$

APPENDIX B: ONE-AXIS TWISTING HAMILTONIAN

Assuming that the resonator frequency ω_R is near resonance with ω_- and the state $|\psi_+\rangle$ is off resonance, the coupling is homogeneous, i.e., $g_n = g$. In this case, we can introduce the collective spin operator, and the total Hamiltonian in Eq. (A11) can be reduced to the following form in the rotating-wave approximation:

$$\hat{H} = \omega_R\hat{a}^\dagger\hat{a} + \omega_-\hat{J}_z + \frac{G}{\sqrt{N}}(\hat{a}\hat{J}^\dagger + \hat{a}^\dagger\hat{J}), \tag{B1}$$

where $\hat{J}_z = \frac{1}{2}\sum_n |\psi_-\rangle_n\langle\psi_-| - |0\rangle_n\langle 0|$ and $\hat{J} = \sum_n |0\rangle_n\langle\psi_-|$ are the collective spin operators satisfying the usual angular momentum commutation relations. Considering the resonator dissipation, the dynamics of total system is described by

$$\dot{\hat{\rho}}_{\text{tot}} = -i[\hat{H}, \hat{\rho}_{\text{tot}}] + (n_{\text{th}}+1)\gamma\mathcal{D}[\hat{a}]\hat{\rho}_{\text{tot}} + n_{\text{th}}\gamma\mathcal{D}[\hat{a}^\dagger]\hat{\rho}_{\text{tot}}, \tag{B2}$$

where $\mathcal{D}[\hat{o}]\hat{\rho} = \hat{o}\hat{\rho}\hat{o}^\dagger - \frac{1}{2}\hat{o}^\dagger\hat{o}\hat{\rho} - \frac{1}{2}\hat{\rho}\hat{o}^\dagger\hat{o}$ is the Lindblad superoperator, $n_{\text{th}} = (e^{kT/\hbar\omega_R}-1)^{-1}$ is the thermal photon number, and γ is the CPW resonator decay rate. The Hamiltonian in Eq. (B1) can be used to model the interaction between a two-level atom ensemble and a single-mode field. Next, we will derive the effective one-axis twisting Lipkin-Meshkov-Glick (LMG) model under the large-detuning condition $G \ll \Delta = \omega_- - \omega_R$. Although discussions similar to what we present here were given in several articles [1,19], we give a detailed derivation to acquire a better understanding. In order to simplify the derivation processes, we rewrite Eq. (B1) in the form of $\hat{H} = \hat{H}_0 + \hat{H}_I$, where $\hat{H}_0 = \omega_R\hat{a}^\dagger\hat{a} + \omega_-\hat{J}_z$ is the free Hamiltonian and $\hat{H}_I = \frac{G}{\sqrt{N}}(\hat{a}\hat{J}^\dagger + \hat{a}^\dagger\hat{J})$ is the interaction Hamiltonian. Applying the Schrieffer-Wolff transformation, $\hat{H} \to \hat{H}_S = e^{\hat{S}}\hat{H}e^{-\hat{S}}$, where $\hat{S}$ has the same order as the interaction term. Expanding the transformation to second order of $\hat{S}$,

$$\begin{aligned}\hat{H}_S &= \hat{H} + [\hat{H},\hat{S}] + \tfrac{1}{2}[[\hat{H},\hat{S}],\hat{S}]\\ &= \hat{H}_0 + \hat{H}_I + [\hat{H}_0+\hat{H}_I,\hat{S}] + \tfrac{1}{2}[[\hat{H}_0+\hat{H}_I,\hat{S}],\hat{S}]\\ &= \hat{H}_0 + (\hat{H}_I + [\hat{H}_0,\hat{S}]) + [\hat{H}_I,\hat{S}] + \tfrac{1}{2}[[\hat{H}_0+\hat{H}_I,\hat{S}],\hat{S}]\\ &= \hat{H}_0 + (\hat{H}_I + [\hat{H}_0,\hat{S}])\\ &\quad + \tfrac{1}{2}[\hat{H}_I,\hat{S}] + \tfrac{1}{2}[(\hat{H}_I + [\hat{H}_0,\hat{S}]),\hat{S}].\end{aligned} \tag{B3}$$

Here, we have neglected the higher-order interactions. Letting $\hat{H}_I + [\hat{H}_0, \hat{S}] = 0$, we can obtain the expression

$$\hat{S} = \frac{g}{\Delta}(\hat{J}\hat{a}^\dagger - \hat{J}^\dagger\hat{a}) \tag{B4}$$

and the final form of the effective total Hamiltonian of Eq. (5) in the main text

$$\hat{H}_S = \omega_R\hat{a}^\dagger\hat{a} + \left(\omega_- + 2\frac{\Lambda}{N}\hat{a}^\dagger\hat{a}\right)\hat{J}_z + \frac{\Lambda}{N}\hat{J}^\dagger\hat{J}, \tag{B5}$$

where we have used the commutation relations $[\hat{J}_+, \hat{J}_-] = 2\hat{J}_z$, $[\hat{J}_z, \hat{J}_+] = \hat{J}_+$. and $[\hat{J}_z, \hat{J}_-] = -\hat{J}_-$ and $\Lambda = G^2/\Delta$ is the spin-spin coupling strength. Because the total spin $\hat{\mathbf{J}}^2$ commutes with the Hamiltonian $\hat{H}_S$, the system evolves within the manifold of $J = N/2$ if the initial state is prepared in the maximally polarized state $|J = N/2, J_x = N/2\rangle$. Assuming the thermal phonon number $n_{\text{th}} \sim 0$, Hamiltonian (B5) in the interaction picture is written as

$$\hat{H}_S = -\frac{\Lambda}{N}\hat{J}_z^2, \tag{B6}$$

which corresponds to the one-axis twisting LMG model and can be used to generate spin-squeezed states. In order to discuss the dissipation dynamics of the spin degrees of freedom, we introduce the reduced density operator $\hat{\rho}$. The evolution of $\hat{\rho}$ is governed by the Born-Markov master equation. Applying the transformation to the master equation and tracing the resonator mode, the dynamics of the reduced density operator $\hat{\rho}$ for spin is described by

$$\dot{\hat{\rho}} = -i[\hat{H}_S, \hat{\rho}] + (n_{\text{th}}+1)\frac{\Gamma}{N}\mathcal{D}[\hat{J}]\hat{\rho} + n_{\text{th}}\frac{\Gamma}{N}\mathcal{D}[\hat{J}^\dagger]\hat{\rho}, \tag{B7}$$

where $\Gamma = \gamma G^2/\Delta^2$.

In the case of inhomogeneous coupling, the Schrieffer-Wolff transform is still valid, with $\hat{S} = \sum_n \frac{g_n}{\Delta}(\hat{\sigma}_n\hat{a}^\dagger - \hat{\sigma}_n^\dagger\hat{a})$.

Then we can get the effective Hamiltonian

$$\hat{H}_S = \sum_n \left(\frac{\Delta}{2} + \frac{g_n^2}{\Delta} \hat{a}^\dagger \hat{a} \right) \hat{\sigma}_n^z + \sum_{n,m} \frac{g_n g_m}{\Delta} \hat{\sigma}_n^\dagger \hat{\sigma}_m, \quad \text{(B8)}$$

where $\hat{\sigma}_n^z = |\psi_-\rangle_n\langle\psi_-| - |0\rangle_n\langle 0|$ is the Pauli operator and $\hat{\sigma}_n = |0\rangle_n\langle\psi_-|$ is the single-spin lowering operator. The corresponding master equation is

$$\dot{\hat{\rho}} = -i[\hat{H}_S, \hat{\rho}] + (n_{\rm th}+1)\frac{\Gamma}{N}\mathcal{D}\left[\sum_n \frac{g_n}{\Delta}\hat{\sigma}_n\right]\hat{\rho} + n_{\rm th}\frac{\Gamma}{N}\mathcal{D}\left[\sum_n \frac{g_n}{\Delta}\hat{\sigma}_n^\dagger\right]\hat{\rho}. \quad \text{(B9)}$$

APPENDIX C: THE VALIDITY OF THE EFFECTIVE HAMILTONIAN

To verify that the effective Hamiltonian and master equation are valid, we compare the results of the original Hamiltonian (B1) (black solid line) and the effective Hamiltonian (B6) (red dashed line) in Fig. 5(a). These two curves fit very well, which means the approximation is valid in our scheme. In addition, the blue dotted line indicates that the photon number is always very small with the chosen parameters. On the other hand, we discuss only the case in which the mean thermal photon number is zero in the main text. Here, we also show the dynamics where the thermal photon number is not zero. The existence of the thermal photon number leads to a reduced degree of squeezing and time for optimal squeezing.

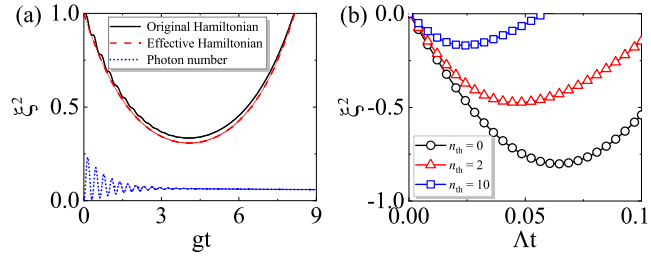

FIG. 5. (a) Evolution of the spin squeezing parameter and photon number. Other parameters are $\Delta/g = 20$, $\gamma/g = 2$, and $N = 10$. (b) Evolution of the spin squeezing parameter with different thermal photon numbers $n_{\rm th} = 0, 2, 10$. Other parameters are $\Gamma/\Lambda = 0.05$ and $N = 50$.

[1] J. Ma, X. Wang, C. Sun, and F. Nori, Quantum spin squeezing, Phys. Rep. **509**, 89 (2011).

[2] A. Sørensen and K. Mølmer, Spin-Spin Interaction and Spin Squeezing in an Optical Lattice, Phys. Rev. Lett. **83**, 2274 (1999).

[3] A. Kuzmich, K. Mølmer, and E. S. Polzik, Spin Squeezing in an Ensemble of Atoms Illuminated with Squeezed Light, Phys. Rev. Lett. **79**, 4782 (1997).

[4] D. J. Wineland, J. J. Bollinger, W. M. Itano, F. L. Moore, and D. J. Heinzen, Spin squeezing and reduced quantum noise in spectroscopy, Phys. Rev. A **46**, R6797 (1992).

[5] D. J. Wineland, J. J. Bollinger, W. M. Itano, and D. J. Heinzen, Squeezed atomic states and projection noise in spectroscopy, Phys. Rev. A **50**, 67 (1994).

[6] A. S. Sørensen and K. Mølmer, Entanglement and Extreme Spin Squeezing, Phys. Rev. Lett. **86**, 4431 (2001).

[7] L. Pezzè, A. Smerzi, M. K. Oberthaler, R. Schmied, and P. Treutlein, Quantum metrology with nonclassical states of atomic ensembles, Rev. Mod. Phys. **90**, 035005 (2018).

[8] H. Bao, J. Duan, S. Jin, X. Lu, P. Li, W. Qu, M. Wang, I. Novikova, E. E. Mikhailov, K.-F. Zhao, K. Mølmer, H. Shen, and Y. Xiao, Spin squeezing of 1011 atoms by prediction and retrodiction measurements, Nature (London) **581**, 159 (2020).

[9] G. Tóth, C. Knapp, O. Gühne, and H. J. Briegel, Spin squeezing and entanglement, Phys. Rev. A **79**, 042334 (2009).

[10] X. Wang and B. C. Sanders, Spin squeezing and pairwise entanglement for symmetric multiqubit states, Phys. Rev. A **68**, 012101 (2003).

[11] J. Geremia, J. K. Stockton, and H. Mabuchi, Real-time quantum feedback control of atomic spin-squeezing, Science **304**, 270 (2004).

[12] S. P. Nolan, S. S. Szigeti, and S. A. Haine, Optimal and Robust Quantum Metrology Using Interaction-Based Readouts, Phys. Rev. Lett. **119**, 193601 (2017).

[13] C. F. Ockeloen, R. Schmied, M. F. Riedel, and P. Treutlein, Quantum Metrology with a Scanning Probe Atom Interferometer, Phys. Rev. Lett. **111**, 143001 (2013).

[14] C. L. Degen, F. Reinhard, and P. Cappellaro, Quantum sensing, Rev. Mod. Phys. **89**, 035002 (2017).

[15] I. Kruse, K. Lange, J. Peise, B. Lücke, L. Pezzè, J. Arlt, W. Ertmer, C. Lisdat, L. Santos, A. Smerzi, and C. Klempt, Improvement of an Atomic Clock Using Squeezed Vacuum, Phys. Rev. Lett. **117**, 143004 (2016).

[16] N. Bigelow, Quantum engineering: Squeezing entanglement, Nature (London) **409**, 27 (2001).

[17] J. K. Korbicz, J. I. Cirac, and M. Lewenstein, Spin Squeezing Inequalities and Entanglement of n Qubit States, Phys. Rev. Lett. **95**, 120502 (2005).

[18] M. Kitagawa and M. Ueda, Squeezed spin states, Phys. Rev. A **47**, 5138 (1993).

[19] S. D. Bennett, N. Y. Yao, J. Otterbach, P. Zoller, P. Rabl, and M. D. Lukin, Phonon-Induced Spin-Spin Interactions in Diamond Nanostructures: Application to Spin Squeezing, Phys. Rev. Lett. **110**, 156402 (2013).

[20] P.-B. Li, Y. Zhou, W.-B. Gao, and F. Nori, Enhancing Spin-Phonon and Spin-Spin Interactions Using Linear Resources in a Hybrid Quantum System, Phys. Rev. Lett. **125**, 153602 (2020).

[21] T. Hernández Yanes, M. Płodzień, M. Mackoit Sinkevičienė, G. Žlabys, G. Juzeliūnas, and E. Witkowska, One- and Two-Axis Squeezing via Laser Coupling in an Atomic Fermi-Hubbard Model, Phys. Rev. Lett. **129**, 090403 (2022).

[22] T. E. Lee, F. Reiter, and N. Moiseyev, Entanglement and Spin Squeezing in Non-Hermitian Phase Transitions, Phys. Rev. Lett. **113**, 250401 (2014).

[23] W. Muessel, H. Strobel, D. Linnemann, D. B. Hume, and M. K. Oberthaler, Scalable Spin Squeezing for Quantum-Enhanced Magnetometry with Bose-Einstein Condensates, Phys. Rev. Lett. **113**, 103004 (2014).

[24] R. J. Lewis-Swan, M. A. Norcia, J. R. K. Cline, J. K. Thompson, and A. M. Rey, Robust Spin Squeezing via Photon-Mediated Interactions on an Optical Clock Transition, Phys. Rev. Lett. **121**, 070403 (2018).

[25] P. Groszkowski, H.-K. Lau, C. Leroux, L. C. G. Govia, and A. A. Clerk, Heisenberg-Limited Spin Squeezing via Bosonic Parametric Driving, Phys. Rev. Lett. **125**, 203601 (2020).

[26] N. Lütkenhaus, J. I. Cirac, and P. Zoller, Mimicking a squeezed-bath interaction: Quantum-reservoir engineering with atoms, Phys. Rev. A **57**, 548 (1998).

[27] E. G. Dalla Torre, J. Otterbach, E. Demler, V. Vuletic, and M. D. Lukin, Dissipative Preparation of Spin Squeezed Atomic Ensembles in a Steady State, Phys. Rev. Lett. **110**, 120402 (2013).

[28] S.-Y. Bai and J.-H. An, Generating Stable Spin Squeezing by Squeezed-Reservoir Engineering, Phys. Rev. Lett. **127**, 083602 (2021).

[29] P. Groszkowski, M. Koppenhöfer, H.-K. Lau, and A. A. Clerk, Reservoir-Engineered Spin Squeezing: Macroscopic Even-Odd Effects and Hybrid-Systems Implementations, Phys. Rev. X **12**, 011015 (2022).

[30] A. S. Parkins, E. Solano, and J. I. Cirac, Unconditional Two-Mode Squeezing of Separated Atomic Ensembles, Phys. Rev. Lett. **96**, 053602 (2006).

[31] J.-Q. Chen, Y.-F. Qiao, X.-L. Dong, X.-L. Hei, and P.-B. Li, Dissipation-assisted preparation of steady spin-squeezed states of SiV centers, Phys. Rev. A **103**, 013709 (2021).

[32] A. González-Tudela and D. Porras, Mesoscopic Entanglement Induced by Spontaneous Emission in Solid-State Quantum Optics, Phys. Rev. Lett. **110**, 080502 (2013).

[33] K. Xia and J. Twamley, Generating spin squeezing states and Greenberger-Horne-Zeilinger entanglement using a hybrid phonon-spin ensemble in diamond, Phys. Rev. B **94**, 205118 (2016).

[34] W. Qin, Y.-H. Chen, X. Wang, A. Miranowicz, and F. Nori, Strong spin squeezing induced by weak squeezing of light inside a cavity, Nanophotonics **9**, 4853 (2020).

[35] P. Cappellaro and M. D. Lukin, Quantum correlation in disordered spin systems: Applications to magnetic sensing, Phys. Rev. A **80**, 032311 (2009).

[36] A. Lenef and S. C. Rand, Electronic structure of the N-*V* center in diamond: Theory, Phys. Rev. B **53**, 13441 (1996).

[37] Y. Doi, T. Fukui, H. Kato, T. Makino, S. Yamasaki, T. Tashima, H. Morishita, S. Miwa, F. Jelezko, Y. Suzuki, and N. Mizuochi, Pure negatively charged state of the NV center in *n*-type diamond, Phys. Rev. B **93**, 081203(R) (2016).

[38] C. Hepp, T. Müller, V. Waselowski, J. N. Becker, B. Pingault, H. Sternschulte, D. Steinmüller-Nethl, A. Gali, J. R. Maze, M. Atatüre, and C. Becher, Electronic Structure of the Silicon Vacancy Color Center in Diamond, Phys. Rev. Lett. **112**, 036405 (2014).

[39] L. J. Rogers, K. D. Jahnke, M. W. Doherty, A. Dietrich, L. P. McGuinness, C. Müller, T. Teraji, H. Sumiya, J. Isoya, N. B. Manson, and F. Jelezko, Electronic structure of the negatively charged silicon-vacancy center in diamond, Phys. Rev. B **89**, 235101 (2014).

[40] I. D. Leroux, M. H. Schleier-Smith, and V. Vuletić, Implementation of Cavity Squeezing of a Collective Atomic Spin, Phys. Rev. Lett. **104**, 073602 (2010).

[41] A. Dantan, J. Cviklinski, E. Giacobino, and M. Pinard, Spin Squeezing and Light Entanglement in Coherent Population Trapping, Phys. Rev. Lett. **97**, 023605 (2006).

[42] L. K. Thomsen, S. Mancini, and H. M. Wiseman, Spin squeezing via quantum feedback, Phys. Rev. A **65**, 061801(R) (2002).

[43] F. Libbi, Pedro Miguel M. C. de Melo, Z. Zanolli, M. J. Verstraete, and N. Marzari, Phonon-Assisted Luminescence in Defect Centers from Many-Body Perturbation Theory, Phys. Rev. Lett. **128**, 167401 (2022).

[44] A. Zobelli, C. P. Ewels, A. Gloter, and G. Seifert, Vacancy migration in hexagonal boron nitride, Phys. Rev. B **75**, 094104 (2007).

[45] L. Weston, D. Wickramaratne, M. Mackoit, A. Alkauskas, and C. G. Van de Walle, Native point defects and impurities in hexagonal boron nitride, Phys. Rev. B **97**, 214104 (2018).

[46] M. Abdi, J.-P. Chou, A. Gali, and M. B. Plenio, Color centers in hexagonal boron nitride monolayers: A group theory and ab initio analysis, ACS Photonics **5**, 1967 (2018).

[47] P. Khatri, A. J. Ramsay, R. N. E. Malein, H. M. H. Chong, and I. J. Luxmoore, Optical gating of photoluminescence from color centers in hexagonal boron nitride, Nano Lett. **20**, 4256 (2020).

[48] X. Gao, S. Pandey, M. Kianinia, J. Ahn, P. Ju, I. Aharonovich, N. Shivaram, and T. Li, Femtosecond laser writing of spin defects in hexagonal boron nitride, ACS Photonics **8**, 994 (2021).

[49] M. E. Turiansky, A. Alkauskas, and C. G. Van de Walle, Spinning up quantum defects in 2D materials, Nat. Mater. **19**, 487 (2020).

[50] S. Baber, R. N. E. Malein, P. Khatri, P. S. Keatley, S. Guo, F. Withers, A. J. Ramsay, and I. J. Luxmoore, Excited state spectroscopy of boron vacancy defects in hexagonal boron nitride using time-resolved optically detected magnetic resonance, Nano Lett. **22**, 461 (2022).

[51] N. Mendelson, R. Ritika, M. Kianinia, J. Scott, S. Kim, J. E. Fröch, C. Gazzana, M. Westerhausen, L. Xiao, S. S. Mohajerani, S. Strauf, M. Toth, I. Aharonovich, and Z.-Q. Xu, Coupling spin defects in a layered material to nanoscale plasmonic cavities, Adv. Mater. **34**, 2106046 (2022).

[52] V. Ivády, G. Barcza, G. Thiering, S. Li, H. Hamdi, J.-P. Chou, Ö. Legeza, and A. Gali, Ab initio theory of the negatively charged boron vacancy qubit in hexagonal boron nitride, npj Comput. Mater. **6**, 41 (2020).

[53] A. Haykal, R. Tanos, N. Minotto, A. Durand, F. Fabre, J. Li, J. H. Edgar, V. Ivády, A. Gali, T. Michel, A. Dréau, B. Gil, G. Cassabois, and V. Jacques, Decoherence of v_b^- spin defects in monoisotopic hexagonal boron nitride, Nat. Commun. **13**, 4347 (2022).

[54] A. Gottscholl, M. Diez, V. Soltamov, C. Kasper, A. Sperlich, M. Kianinia, C. Bradac, I. Aharonovich, and V. Dyakonov, Room temperature coherent control of spin defects in hexagonal boron nitride, Sci. Adv. **7**, eabf3630 (2021).

[55] W. Liu, Z.-P. Li, Y.-Z. Yang, S. Yu, Y. Meng, Z.-A. Wang, Z.-C. Li, N.-J. Guo, F.-F. Yan, Q. Li, J.-F. Wang, J.-S. Xu, Y.-T. Wang, J.-S. Tang, C.-F. Li, and G.-C. Guo, Temperature-dependent energy-level shifts of spin defects in hexagonal boron nitride, ACS Photonics **8**, 1889 (2021).

[56] N. Chejanovsky, A. Mukherjee, J. Geng, Y.-C. Chen, Y. Kim, A. Denisenko, A. Finkler, T. Taniguchi, K. Watanabe, D. B. R. Dasari, P. Auburger, A. Gali, J. H. Smet, and J. Wrachtrup,

Single-spin resonance in a van der Waals embedded paramagnetic defect, Nat. Mater. **20**, 1079 (2021).

[57] F. F. Murzakhanov, G. V. Mamin, S. B. Orlinskii, U. Gerstmann, W. G. Schmidt, T. Biktagirov, I. Aharonovich, A. Gottscholl, A. Sperlich, V. Dyakonov, and V. A. Soltamov, Electron–nuclear coherent coupling and nuclear spin readout through optically polarized V_B^- spin states in hBn, Nano Lett. **22**, 2718 (2022).

[58] A. Gottscholl, M. Kianinia, V. Soltamov, S. Orlinskii, G. Mamin, C. Bradac, C. Kasper, K. Krambrock, A. Sperlich, M. Toth, I. Aharonovich, and V. Dyakonov, Initialization and read-out of intrinsic spin defects in a van der Waals crystal at room temperature, Nat. Mater. **19**, 540 (2020).

[59] F. F. Murzakhanov, B. V. Yavkin, G. V. Mamin, S. B. Orlinskii, I. E. Mumdzhi, I. N. Gracheva, B. F. Gabbasov, A. N. Smirnov, V. Y. Davydov, and V. A. Soltamov, Creation of negatively charged boron vacancies in hexagonal boron nitride crystal by electron irradiation and mechanism of inhomogeneous broadening of boron vacancy-related spin resonance lines, Nanomaterials **11**, 1373 (2021).

[60] M. Kianinia, S. White, J. E. Fröch, C. Bradac, and I. Aharonovich, Generation of spin defects in hexagonal boron nitride, ACS Photonics **7**, 2147 (2020).

[61] N.-J. Guo, W. Liu, Z.-P. Li, Y.-Z. Yang, S. Yu, Y. Meng, Z.-A. Wang, X.-D. Zeng, F.-F. Yan, Q. Li, J.-F. Wang, J.-S. Xu, Y.-T. Wang, J.-S. Tang, C.-F. Li, and G.-C. Guo, Generation of spin defects by ion implantation in hexagonal boron nitride, ACS Omega **7**, 1733 (2022).

[62] T. Yang, N. Mendelson, C. Li, A. Gottscholl, J. Scott, M. Kianinia, V. Dyakonov, M. Toth, and I. Aharonovich, Spin defects in hexagonal boron nitride for strain sensing on nanopillar arrays, Nanoscale **14**, 5239 (2022).

[63] A. Gottscholl, M. Diez, V. Soltamov, C. Kasper, D. Krauße, A. Sperlich, M. Kianinia, C. Bradac, I. Aharonovich, and V. Dyakonov, Spin defects in hBn as promising temperature, pressure and magnetic field quantum sensors, Nat. Commun. **12**, 4480 (2021).

[64] P. Kumar, F. Fabre, A. Durand, T. Clua-Provost, J. Li, J. H. Edgar, N. Rougemaille, J. Coraux, X. Marie, P. Renucci, C. Robert, I. Robert-Philip, B. Gil, G. Cassabois, A. Finco, and V. Jacques, Magnetic Imaging with Spin Defects in Hexagonal Boron Nitride, Phys. Rev. Appl. **18**, L061002 (2022).

[65] L. Gan, D. Zhang, R. Zhang, Q. Zhang, H. Sun, Y. Li, and C.-Z. Ning, Large-scale, high-yield laser fabrication of bright and pure single-photon emitters at room temperature in hexagonal boron nitride, ACS Nano **16**, 14254 (2022).

[66] X. Gao, B. Jiang, A. E. Llacsahuanga Allcca, K. Shen, M. A. Sadi, A. B. Solanki, P. Ju, Z. Xu, P. Upadhyaya, Y. P. Chen, S. A. Bhave, and T. Li, High-contrast plasmonic-enhanced shallow spin defects in hexagonal boron nitride for quantum sensing, Nano Lett. **21**, 7708 (2021).

[67] D. Curie, J. T. Krogel, L. Cavar, A. Solanki, P. Upadhyaya, T. Li, Y.-Y. Pai, M. Chilcote, V. Iyer, A. Puretzky, I. Ivanov, M.-H. Du, F. Reboredo, and B. Lawrie, Correlative nanoscale imaging of strained hBn spin defects, ACS Appl. Mater. Interfaces **14**, 41361 (2022).

[68] J. Verdú, H. Zoubi, C. Koller, J. Majer, H. Ritsch, and J. Schmiedmayer, Strong Magnetic Coupling of an Ultracold Gas to a Superconducting Waveguide Cavity, Phys. Rev. Lett. **103**, 043603 (2009).

[69] Z.-L. Xiang, S. Ashhab, J. Q. You, and F. Nori, Hybrid quantum circuits: Superconducting circuits interacting with other quantum systems, Rev. Mod. Phys. **85**, 623 (2013).

[70] S. Cohn, Slot-line field components (correspondence), IEEE Trans. Microwave Theory Tech. **20**, 172 (1972).

[71] Y. Kubo, F. R. Ong, P. Bertet, D. Vion, V. Jacques, D. Zheng, A. Dréau, J.-F. Roch, A. Auffeves, F. Jelezko, J. Wrachtrup, M. F. Barthe, P. Bergonzo, and D. Esteve, Strong Coupling of a Spin Ensemble to a Superconducting Resonator, Phys. Rev. Lett. **105**, 140502 (2010).

[72] P. Rabl, P. Cappellaro, M. V. Gurudev Dutt, L. Jiang, J. R. Maze, and M. D. Lukin, Strong magnetic coupling between an electronic spin qubit and a mechanical resonator, Phys. Rev. B **79**, 041302(R) (2009).

[73] P.-B. Li, Y.-C. Liu, S.-Y. Gao, Z.-L. Xiang, P. Rabl, Y.-F. Xiao, and F.-L. Li, Hybrid Quantum Device Based on *NV* Centers in Diamond Nanomechanical Resonators Plus Superconducting Waveguide Cavities, Phys. Rev. Appl. **4**, 044003 (2015).

[74] D. Bothner, D. Wiedmaier, B. Ferdinand, R. Kleiner, and D. Koelle, Improving Superconducting Resonators in Magnetic Fields by Reduced Field Focussing and Engineered Flux Screening, Phys. Rev. Appl. **8**, 034025 (2017).

[75] J. R. Schrieffer and P. A. Wolff, Relation between the Anderson and Kondo Hamiltonians, Phys. Rev. **149**, 491 (1966).

[76] W. Song, W. Yang, J. An, and M. Feng, Dissipation-assisted spin squeezing of nitrogen-vacancy centers coupled to a rectangular hollow metallic waveguide, Opt. Express **25**, 19226 (2017).

[77] J. Du, X. Rong, N. Zhao, Y. Wang, J. Yang, and R. B. Liu, Preserving electron spin coherence in solids by optimal dynamical decoupling, Nature (London) **461**, 1265 (2009).

[78] W. Liu *et al.*, Coherent dynamics of multi-spin V_B^- center in hexagonal boron nitride, Nat. Commun. **13**, 5713 (2022).

[79] A. Blais, R.-S. Huang, A. Wallraff, S. M. Girvin, and R. J. Schoelkopf, Cavity quantum electrodynamics for superconducting electrical circuits: An architecture for quantum computation, Phys. Rev. A **69**, 062320 (2004).

[80] B. Yurke and J. S. Denker, Quantum network theory, Phys. Rev. A **29**, 1419 (1984).

[81] J. R. Johansson, G. Johansson, C. M. Wilson, and F. Nori, Dynamical Casimir effect in superconducting microwave circuits, Phys. Rev. A **82**, 052509 (2010).